Understanding Arsenic Incorporation in CdTe with Atom Probe Tomography

G. L. Burton[1], D. R. Diercks[1], O. S. Ogedengbe[2], P. A. Jayathilaka[2], M. Edirisooriya[2], T.H. Myers[2], K. Zaunbrecher[3,4], J. Moseley[3], T. Barnes[3], and B. P. Gorman[1]

[1]*George S. Ansell Department of Metallurgical and Materials Engineering, Colorado School of Mines, Golden, CO 80401, USA*

[2]*Materials Science, Engineering, and Commercialization Program, Texas State University, 601 University Dr., San Marcos, Texas 78666, USA*

[3]*National Renewable Energy Laboratory, 15013 Denver West Parkway, Golden, Colorado 80401, USA*

[4]*Department of Physics, Colorado State University, Fort Collins, CO, 80526, USA*

Abstract

Overcoming the open circuit voltage deficiency in Cadmium Telluride (CdTe) photovoltaics may be achieved by increasing p-type doping while maintaining or increasing minority carrier lifetimes. Here, routes to higher doping efficiency using arsenic are explored through an atomic scale understanding of dopant incorporation limits and activation in molecular beam epitaxy grown CdTe layers. Atom probe tomography reveals spatial segregation into nanometer scale clusters containing >60 at% As for samples with arsenic incorporation levels greater than 7-8 x 10^{17} cm^{-3}. The presence of arsenic clusters was accompanied by crystal quality degradation, particularly the introduction of arsenic-enriched extended defects. Post-growth annealing treatments are shown to increase the size of the As precipitates and the amount of As within the precipitates.

Keywords: CdTe; As doping; Atom probe tomography; Scanning transmission electron microscopy; Molecular beam epitaxy; single crystalline

1. Introduction

Pursuant to the DOE Public Access Plan, this document represents the authors' peer-reviewed, accepted manuscript. The published version of the article is available from the relevant publisher.

Thin film polycrystalline Cadmium Telluride (CdTe) photovoltaics have shown exceptional promise reaching efficiencies of over 20% [1]. With the short circuit current (J_{sc}) practically at its fundamental threshold, the limiting factor in further advancing the efficiency of CdTe devices towards its theoretical limits is the open-circuit voltage (V_{oc}), which has stayed comparatively unchanged [2,3]. Increasing the p-type doping limit without compromising minority carrier lifetime is essential in overcoming this V_{oc} deficiency. Even though copper (Cu) is typically used as the p-type dopant in polycrystalline CdTe devices and high incorporation values are possible, the activation of Cu in CdTe is quite low, resulting in maximum obtainable carrier concentrations on the order of 10^{15} cm^{-3} [4].

In general, extrinsic p-type doping in CdTe can be achieved by replacing Cd with group I elements under Te-rich conditions or by replacing Te with group V elements under Cd-rich conditions. The diffusion of group I elements in CdTe is significantly faster than group V [5]. Additionally, under Te-rich environments, the Tellurium antisite (Te_{Cd}) defect is readily created and it has been shown experimentally and theoretically that the antisite defect acts as a major recombination center, therefore lowering minority carrier lifetime [6]. Thus, growth under Cd-rich conditions using group V dopants should be more favorable for increasing V_{oc}. Indeed a device made with a phosphorous (P) doped CdTe single crystal absorber, processed under Cd rich conditions, surpassed hole concentrations of 1×10^{17} cm^{-3} and yielded a $V_{oc} > 1$ V [7]. In addition to P as a potentially successful group V dopant, Density Functional Theory (DFT) calculations predicts arsenic (As) to also be a good alternative to Cu due to a similarly low defect formation energy, shallow acceptor level and lower diffusion rate [8]. While P has a lower ionization energy and predicted lower affinity for AX center formation compared to As, arsenic is considered to be a safer option for large-scale production and has a slower diffusion mechanism than phosphorous [9,10].

Arsenic doping of CdTe alloys has been an area of active research for many years, particularly for mercury cadmium telluride (HgCdTe) alloys in infrared devices [5,11–13]. However, there are many challenges associated with As doping in CdTe, especially difficulties associated with dopant activation

Pursuant to the DOE Public Access Plan, this document represents the authors' peer-reviewed, accepted manuscript. The published version of the article is available from the relevant publisher.

[14,15]. As-grown films are typically highly compensating, meaning that the obvious scenario under a Cd rich growth environment for which As is primarily incorporated onto a vacant tellurium site is not the case. Post-growth annealing procedures at high temperature are necessary to properly activate the As dopants, [13,16] and the mechanism for activation in CdTe is not well established. In HgCdTe, the commonly cited mechanism [17–20] for activation involves growth under a Te rich environment, prompting the amphoteric dopant, As, to sit on a Hg or Cd site. A high temperature activation anneal, typically an ampoule anneal under Te overpressure, allows As to migrate to a Te vacancy (V_{Te})site. Nevertheless, other theories for As:HgCdTe activation exist [13] including one with experimental evidence showing the formation of an $AsHg_8$ complex and As_2Te_3 glass [21–23]. Since HgCdTe is grown under Te-rich environments, the mechanism for CdTe grown under Cd-rich conditions should be different. The present study examines two annealing methods, ampoule to facilitate comparison with success in HgCdTe annealing, and rapid thermal processing (RTP)[24], a technique used frequently in semiconductor manufacturing to activate dopants, and has been used previously for CdTe samples[25].

Another problem with As activation involves the drop in net acceptor density at high incorporation levels of As [26–29] which is typically attributed to AX formation [30–33]. The AX compensating donor defect is formed by As breaking two bonds with Cd so that the As atom can move toward the neighboring Te atom and form an As-Te bond. Experimental evidence of the AX center was recently shown to most likely be the dominant donor compensating defect via thermoelectric-effect spectroscopy (TEES) [34]. An alternative or competing phenomenon could also be contributing to compensation at high As concentrations, especially approaching the solubility of As in CdTe: the formation of As-related clusters. The formation of secondary phases in CdTe has been reported previously for a limited number of dopants [35]. Duan et al., using density functional theory (DFT), suggest that the solubility of As in HgCdTe is mainly controlled by the precipitation of elemental As clusters, or under Te rich environments, an As_2Te_3 compound [36]. There are a few experimental observations that discuss the possible formation of these As-related clusters. In a CdTe sample with As concentrations of 1.5×10^{19} cm^{-3}, preliminary x-ray

Pursuant to the DOE Public Access Plan, this document represents the authors' peer-reviewed, accepted manuscript. The published version of the article is available from the relevant publisher.

diffraction (XRD) data shows the possibility of As_2Te_3 formation [37]. Arsenic cluster formation associated with an As_2Te_3 glass was found to exist via extended x-ray absorption fine structure (EXAFES) in As:HgCdTe [22]. After annealing, the glass dissociated, but at higher dopant concentrations (> 2 x10^{18} cm^{-3}), the signal was saturated by the As_2Te_3 glass or other As related clusters [38]. Clusters associated with As and H were found by SIMS ionic imaging in highly doped CdTe samples grown by MOVPE [39]. Larger As-dopant related clusters were also found via IR microscopy in a different study that may have contributed to the low level of dopant incorporation [34].

In the present investigation, atom probe tomography (APT) is employed for the direct nanoscale three-dimensional visualization of the As distribution in heavily As-doped CdTe. This is possible due to the remarkable spatial resolution and chemical sensitivity of the instrument, which has routinely investigated dopant segregation and clustering in other semiconductors [40] as well as a number of additional classes of materials. The effect of various annealing conditions on these highly doped samples is also explored. These findings will help to develop a comprehensive picture of compensation and activation in p-type doped CdTe.

2. Experimental Details

As-doped CdTe samples were grown in a custom molecular beam epitaxy (MBE) system using a recipe that has previously been described [41]. Due to its negligible lattice mismatch and previous success, InSb was used as the substrate on which a 500 nm CdTe buffer layer was grown prior to the As-doped CdTe growth. A solid-source Cd_3As_2 effusion cell was used for As doping in this work, and a 20% Cd overpressure was applied to improve As incorporation [15]. As-doped CdTe layers were grown at a constant Cd_3As_2 to CdTe beam equivalent pressure (BEP) at a constant 205°C substrate temperature. Two different annealing methods were used to activate As dopants. Ampoule annealing occurred in a sealed quartz ampoule under a Cd overpressure in a clam-shell furnace. RTP annealing occurred under an argon atmosphere with samples placed face down on a clean Si substrate.

Pursuant to the DOE Public Access Plan, this document represents the authors' peer-reviewed, accepted manuscript. The published version of the article is available from the relevant publisher.

Cathodoluminescence spectrum imaging (CLSI) was conducted on the top surfaces of films with a Horiba H-CLUE CL system in a JEOL 7600F Schottky Field-Emission SEM. In CLSI, a full luminescence spectrum comparable to photoluminescence spectra is collected at each pixel in an SEM image. Samples were cooled to a temperature of 6 K using a continuous-flow liquid-helium cold stage (Gatan CF302). Electron-beam conditions of 5-kV accelerating voltage and 1-nA current were used, giving a generation depth of about 100-200 nm [42]. Spectra were not corrected for the CL system spectral response, and the CLSI false-color maps (explained below) contain 200×200 pixels.

Secondary ion mass spectrometry (SIMS) measurements were performed to compare the global As concentration profile to the nanoscale As concentration measured by APT. Atom probe specimens were prepared with an FEI Helios 600i DualBeam focused ion beam/scanning electron microscope (FIB/SEM) [43]. Final specimen radii varied between 50-100 nm after a 2 kV cleaning procedure to reduce gallium ion damage to roughly 2 nm on the surface. APT measurements were taken using a Cameca Instruments LEAP 4000X Si. During data collection, a charge state ratio for Cd^{+}/Cd^{2+} around 15 was maintained, typically associated with a laser energy of ~6 pJ and base temperature of ~24 K, following previous work in CdTe running parameters [44]. A 250 kHz laser pulse rate was used and a 4% detection rate could typically be achieved. Due to the relatively small amount of As in these As-doped CdTe samples, the running parameters for As-doped CdTe should not drastically differ from pure CdTe so no additional study of running parameters was performed. To more accurately calibrate the reconstructions of the APT data, transmission electron microscope (TEM) images were acquired prior to and following APT measurements using a Philips CM200 TEM [45,46]. High-angle annular dark-field (HAADF) imaging and EDS mapping was performed on an FEI Co. Talos F200X Scanning Transmission Electron Microscope (STEM) equipped with ChemiSTEM™ capabilities and operated at 200keV.

Pursuant to the DOE Public Access Plan, this document represents the authors' peer-reviewed, accepted manuscript. The published version of the article is available from the relevant publisher.

3. Results and Discussion

3.1 Arsenic dopant activation below solubility limit

3.1.1 Cathodoluminescence spectrum imaging

Epilayers with lower doping profiles, with an As concentration of about 3.5×10^{16} cm^{-3} measured by SIMS before annealing, were examined to demonstrate As dopant incorporation and activation below the solubility limit. CLSI results conducted on an As-doped CdTe sample before and after rapid thermal processing (RTP) annealing are shown in Figure 1(a)-(b) and Figure 1(c)-(d), respectively. In each figure we show an SEM image and the average CL spectrum over the entire scanned area. CLSI false color maps can be found in supplimental info, showing uniformity across the two samples. Deviations were found at surface impurities (hillocks, debris, etc.) It can be seen that the peaks labeled 1 and 3 in Figs. 1(d) and 2(d) have similar energies. The energies of peaks 1 and 3 agree well with low-temperature photoluminescence literature values of bound exciton and DAP transitions involving As_{Te} acceptors of 1.5987 and 1.510 eV, respectively [10]. However, the relatively high intensity for peak 2 before annealing (Fig. 1(d)) is typical of undoped CdTe. In addition, distinct phonon replica for the deep donor-acceptor pair (DAP) transitions are only seen after annealing (Fig. 2(d) peaks 4 and 5). The average CL spectrum results indicate that for the annealed sample all As has been activated onto Te sites.

3.2 Visualization and analysis of As-related clustering

3.2.1 Atom probe tomography

For this study, a CdTe sample with a 5×10^{19} cm^{-3} As concentration was analyzed at various annealing conditions: unannealed, ampoule anneal, RTP at 550°C, and RTP at 600°C. The thickness of the As-doped layer was roughly 1 μm. The sample was then broken into multiple sections and three of these sections were annealed using different ambients, temperatures, and heating rates to compare chemical changes with electrical activation of As. One piece was annealed in a sealed quartz ampoule under a Cd overpressure in a clam-shell furnace at 450 °C for 10 min. Two pieces were annealed by RTP, one at 550

Pursuant to the DOE Public Access Plan, this document represents the authors' peer-reviewed, accepted manuscript. The published version of the article is available from the relevant publisher.

°C and one at 600 °C. RTP annealing occurred under an argon atmosphere with samples placed face down on a clean Si substrate.

For all annealing conditions, such high levels of As in the CdTe matrix were found to lead to severe crystal degradation and substantial reduction in hole carrier concentrations, as has been seen for MBE-grown CdTe samples under similar conditions [14,15,47]. Structural degradation was always accompanied by rapid increase in As flux of 1 x 10^3 during MBE growth. This phenomenon can be referred to as a runaway postive feedback effect for which the degraded structure allows for more As incorporation into the crystal lattice. The As-concentration profiles for these samples as determined by SIMS can be seen in Figure 2a, where the 500 nm undoped CdTe layer is located 1 μm from the top surface. The unannealed sample has a relatively flat concentration profile of As concentration ~1 x 10^{19} – 1 x 10^{20} cm^{-3}, but there is some As accumulation at the undoped CdTe layer interface. Ampoule annealing causes As to diffuse into the undoped CdTe layer prompting a reduction in the overall concentration of As in the doped layer, however, the concentration profile keeps a similar shape as the unannealed sample. RTP annealing at 600°C causes rapid diffusion, with both a large amount of surface depletion and diffusion into the undoped CdTe layer and even the substrate. These two factors contribute to a large peak in As concentration to 6.2 x 10^{19} cm^{-3} around 0.65 μm depth.

When looking at chemical information at the nanoscale for the same group of samples, atom probe results (Figure 3) show spatial segregation of As into clusters ranging from a few to hundreds of nm^3 in size. The purple 3.2 % isoconcentration surfaces, in which the objects contain 3.2 at. % or greater As, highlight where As clustering is occuring. 3D reconstructions of the unannealed (Figure 3a), ampoule annealed (Figure 3b), RTP 550 °C annealed (Figure 3c) and RTP 600 °C annealed (Figure 3d) samples show a drastic difference in the number of arsenic clusters. 1D compositional profiles down the z-axis for all four annealing conditions, shown in Figure 2b, were performed to compare the compositional changes from APT at one small cross-section in the sample with the overall arsenic concentration obtained by SIMS.

Pursuant to the DOE Public Access Plan, this document represents the authors' peer-reviewed, accepted manuscript. The published version of the article is available from the relevant publisher.

There is some error associated with determining the location of the specimen surface in the APT measurement, since no fiducial was created. However, the shift in the APT z-axis would be at most 50 nm in the positive x direction. Concentration values are quantified after subtracting the background, which was ranged at regions directly adjacent to and at the same mass-to-charge width as the corresponding As peaks in the APT mass spectrum. The APT-measured arsenic concentration for the unannealed sample is more than two times smaller than values given by SIMS, although the relatively flat profile for the first 550 nm is consistent with SIMS. RTP 550 °C and RTP 600 °C annealed samples have a similar maximum in As concentration around 600-700 nm. While the chemical sensitivity of the APT measurement is reduced at the specimen surface due to the needle-like specimen geometry, there is no sign of surface depletion which is seen in the SIMS results. The ampoule annealed sample has a much higher concentration as measured by APT and does not have a distinct maximum in contrast to the SIMS results. Overall, the differences found between the APT and SIMS data indicate that there are significant spatial inhomogenieties, which will be discussed more in depth later.

Inspecting the APT reconstructions in more detail, the unannealed sample, Figure 3a, shows small As clusters relatively evenly dispersed throughout the specimen. The RTP 550 °C annealed sample reveals larger clusters 600-800 nm from the surface of the specimen, which are fewer in number and larger than the unannealed sample. In the RTP 600 °C annealed sample there are fewer clusters >15 nm^3 compared to the RTP 550 °C annealed sample, most likely due to a more rapid diffusion of As into the substrate and a lower overall arsenic concentration in the RTP 600 °C annealed sample. Ampoule annealing (Figure 3b) exhibits a much greater volume of As clustering. Overall, the As concentration is greater than the other 3 samples as described previously. Inspecting the As isoconcentration surfaces of the ampoule annealed sample more closely, the arsenic appears to be in 2D planar structures as shown in Figure 3e and 3f. This phenomenon may be due to As segregating preferentially to structural defects such as stacking faults and dislocations.

Pursuant to the DOE Public Access Plan, this document represents the authors' peer-reviewed, accepted manuscript. The published version of the article is available from the relevant publisher.

To better understand the composition changes within these As clusters, 1D concentration profiles through one cluster in each sample was performed. This measurement was accomplished by defining a cylindrical region of interest with a diameter of ~3 nm whose center was aligned with the center of the cluster of interest. Every ion within the cylinder was counted and assigned its corresponding chemical species. An example cylindrical region can be found in Figure 4a. 1D profiles for the unannealed (Figure 4b), 550 °C annealed sample (Figure 4c), and 600 °C annealed sample (Figure 4d), show As concentrations of around 60, 55, and 70 atomic %, respectively, within the As clusters. The largest cluster in each sample was chosen for these analyses, so not all clusters in the samples show these levels of As. There may also be some effects of local magnification on the measured As concentration in the clusters [48]. Local magnification effects in APT occur when precipitates have a different evaporation field than the matrix. When a precipitate has a higher evaporation field than the matrix, the more commonly used APT reconstruction procedure, integrated in IVAS using a hemispherical tip shape, compensates for the lower density by compressing the volume of the precipitate in the depth direction, which was observed for the As precipitates [49]. This can lead to biases in the concentration profiles since bins can overlap and average out differences, but these differences will be minor. From the information in Figure 3 and 4, we can deduce that while the unannealed sample has more evenly dispersed clusters, the RTP 600°C annealed sample should have more As within a given cluster.

A detailed analysis of the As clusters was performed for all anneal conditions to determine the average cluster size and the overall concentration of As inside and outside of clusters. For the average cluster volume analysis whose results are shown in column 4 of Table I, As clusters associated with the background down the central axis due to the detector configuration were exlcuded. Additionally, for the 600°C RTP sample, there was an increase in As concentration at one surface of the reconstruction, which was assoicated with density fluctuations and were exluded. Finally, clusters <2 nm^3 were removed from this analysis due to possible errors in the reconstruction. To measure the concentration inside and outside the As clusters, first the background in the APT mass spectrum was ranged at regions directly adjacent to

Pursuant to the DOE Public Access Plan, this document represents the authors' peer-reviewed, accepted manuscript. The published version of the article is available from the relevant publisher.

and at the same mass-to-charge widths as the corresponding As peaks (As, As_2, AsTe, and As_4 were observed). The total As concentration was then calculated after the ranged background was subtracted from the total As counts. This can be compared to the average SIMS concentration in column one of Table I, which was calculated by averaging all data points within the same distance that was analyzed for the respective APT specimens. Again, there is a significant difference between the concentrations as measured by the two techniques. Next, the higher As concentration side of 3.2% were created and subsequently excluded from the dataset. The concentration of As outside the clusters could then be calculated from the newly created volume. Arsenic concentrations inside the clusters were calculated by subtracting the outside concentration from the total concentration of As.

Comparing the annealed and unannealed samples, there is a general increase in the cluster size and an increase in the concentration of As inside the clusters with more aggressive annealing. From Table I, the ampoule annealed sample produced an increase in the cluster size compared to the unannelaed case, from 28.05 nm^3 to 49.58 nm^3. And a greater percentage of As, from 24.65% to 42.99%, seems to reside in clusters as compared to the unannealed case. The changes in cluster size and As cluster concentration are much less drastic than those for the RTP samples, a result in agreement with the SIMS analyses. The RTP samples saw an increase of cluster size to 116.6 nm^3 and 125.1 nm^3 and cluster concentrations grew to 82.2% and 93.33% of the total As concentration within the 550°C and 600°C RTP samples, respectively. An increase in size and concentration of the As clusters after undergoing an anneal suggests Ostwald ripening, in which As is diffusing and segregating even more to form larger, higher concentration clusters.

3.2.2 Scanning Transmission Electron Microscopy

Arsenic cluster formation was independently verified by HAADF STEM imaging using the RTP 550 °C annealed sample. The APT specimen, shown in Figure 5a, appears to have regions of darker contrast. In HAADF images, the intensity is approximately proportional to the square of the atomic number, Z. Therefore, the darker regions in the image have a lower average atomic number, which could be

Pursuant to the DOE Public Access Plan, this document represents the authors' peer-reviewed, accepted manuscript. The published version of the article is available from the relevant publisher.

explained by an enrichment of arsenic. To test this hypothesis, a portion of the APT specimen was selected for energy-dispersive x-ray spectroscopy (EDS) mapping, denoted by the blue box in Figure 7a. The HAADF image of the smaller area is shown in Figure 5b, where the darker regions have been circled for clarity. The darker circled regions are between 15-30 nm in diameter, which agrees well with the average volume of arsenic clusters calculated for the RTP 550 °C annealed sample found in Table I. The arsenic EDS map of the same area as Figure 5b is found in Figure 5c. The circled regions do show signs of an increase in As concentration, particularly the red dashed features. After further quantitative analysis, it was found that the red dashed features contained ~4 at. % As, while being slightly enriched in Te and deficient in Cd. The white dotted areas were ~1 at. % As, slightly enriched in Cd, and deficient in Te. In the HAADF images, the white dotted areas are just as dark, if not darker than the red dashed areas, which makes sense since $Z_{Cd} < Z_{Te}$. The values of As in the clusters are significantly lower than those found with APT, and is most likely due to the larger interaction volume and thickness of the sample. Since the clusters are roughly 20 nm in diameter, and the thickness of the APT specimen in that region is ~150 nm, the EDS signal is collecting concentration information not only from the clusters but also the surrounding matrix. APT was used to try to verify if there were indeed two different types of clusters, Te rich and Cd rich, but only slightly Cd rich or equally Cd and Te depleted clusters were found. Ongoing work is being done to understand these clustering differences.

Three-dimensional time of flight-secondary ion mass spectrometry (TOF-SIMS) imaging was also used to try to verify the existence of these As clusters. TOF-SIMS imaging has been used previously in polycrystalline CdTe to visualize dopant segregation to grain boundaries [9,50]. However, no clustering was found in these highly-doped As:CdTe single crystal samples, due to the technique's limited spatial resolution. Low-temperature CLSI imaging conducted on this sample showed low intensities and a broad band with a peak energy of ~1.47 eV. This is consistent with the Y-luminescence band, which is due to extended defects [51].

Pursuant to the DOE Public Access Plan, this document represents the authors' peer-reviewed, accepted manuscript. The published version of the article is available from the relevant publisher.

3.3 Solubility Limit

While solubility does depend on growth conditions, general conclusions can still be made about arsenic in CdTe. After analyzing a number of As-doped CdTe samples with both SIMS and APT, it would seem that the limit to arsenic incorporation before detrimental clusters begin to form is between 7-8 x 10^{17} cm^{-3}. Although no visible clustering is seen, even samples with 8 x 10^{17} cm^{-3} As incorporated, there is a slight preference for As to preferentially segregate as evaluated by nearest neighbor distributions in the APT datasets [52]. The concentration of arsenic outside the clusters in the RTP 600 °C annealed sample corresponds to 2.65 x 10^{17} cm^{-3}, which matches well with the range where no detrimental clusters form. It is believed that the solubility limit could be extended past the range stated above with annealing, as long as the cluster size and concentrations are fairly low. As has been previously reported by EXAFS, annealing can eliminate As_2Te_3 clusters in HgCdTe, as long as the clusters are below a certain size [22]. It is reasonable then to suggest that this phenomenon is possible with As-doped CdTe, although more research must be done to verify this.

3.4 Cluster formation

From Figure 6b-d, both Cd and Te seem to be replacing As at near equal amounts. This contradicts previous related results [15,52,53] that showed more Cd than Te being replaced by As, which led to speculation that the clusters were As_2Te_3 precipitates. This could have been due to different processing conditions since the samples were prepared in a different MBE system, using a thermal cracker for As_2 production rather than a solid source Cd_3As_2 effusion cell as done in the current study. Given that the samples were grown in a Cd-rich growth environment, following calculations from Duan et al. [36], at high enough As concentrations, elemental As precipitates could form. If most or all V_{Te} have been filled, As_{Cd} antisites or arsenic interstitials (As^i) could form even given their higher formation energies compared to As_{Te}. The As_{Cd} and As^i defects can then cluster together as in the HgCdTe case where As_{Hg} and As^i defects would cluster [36]. It should be noted that APT also discovered ~1 at.% oxygen and nitrogen cluster formation particulary in the annealed samples but this will be the topic of a future study.

Pursuant to the DOE Public Access Plan, this document represents the authors' peer-reviewed, accepted manuscript. The published version of the article is available from the relevant publisher.

These highly As-doped CdTe samples have proven to be highly non-uniform laterally, confirmed by comparison with SIMS and APT data in the present study. APT specimens were found to either exhibit much higher or much lower concentrations compared with SIMS. In addition, not shown in this report, APT specimens prepared 5 μm apart in the same liftout have exhibited drastically different arsenic behavior, one specimen with an elevated As concentration compard with SIMS and the other with an As concentration that could not be detected within the limits of the atom probe measurement. This phenomenon can be attributed to non-uniformities in defect distribution and, subsequently, preferential segregation of As to these stacking faults and dislocations, which accounts for the planar structures in the ampoule annealed sample. The concentration of As in the ampoule annealed sample is also two times higher as measured by APT when compared to the SIMS result (Table I and Figure 4). It is believed that arsenic accumulation on the growing surface of the sample at some critical density nucleates arsenic precipitation, causing structural defects and allowing an increase in As incorporation to these defects. This explains the runaway positive feedback mentioned previously.

3.5 Dopant Activation

Arsenic cluster formation can be compared with dopant activation from Figure 3. These precipitates provide a compensation mechanism to further decrease the hole carrier concentrations even more so than what has been seen for AX center formation. Once clusters start forming, fewer dopants are activated because they are no longer part of the CdTe crystal. Then as the percentage of As in clusters grows, this becomes even more pronounced. The activation versus concentration curve, as has been seen previously[29] suggests that beyond a certain dopant level, adding more dopant actually takes away activated species. AX center formation causes a decrease in carrier activation without appreciable clustering, but after further arsenic incorporation, As cluster formation further decreases carrier activation. With increasing arsenic incorporation, the solubility limit of arsenic in CdTe is reached causing the formation of As clusters.

Pursuant to the DOE Public Access Plan, this document represents the authors' peer-reviewed, accepted manuscript. The published version of the article is available from the relevant publisher.

4. Conclusion

In conclusion, As:CdTe epitaxial layers grown by MBE under a Cd-rich environment were carried out to investigate the distribution of As in CdTe and its effects on performance. Low temperature CLSI indicates the full activation of As_{Te} and the uniformity of doping after a high temperature anneal of a sample with 10^{16} cm^{-3} As incorporation. Highly As doped CdTe samples with concentrations > 1 x 10^{19} cm^{-3} arsenic were also examined by SIMS and APT under a number of annealing conditions. APT results found preferential segregation of As in these samples to form As-rich precipitates contributing to structural degradation and contributing to the reduction in hole concentrations. Precipitates in the annealed samples grew larger and became richer in arsenic. Samples were found to be spatially inhomogeneous with respect to arsenic concentration, possibly due to the preferential segregation to stacking faults and dislocations.

Acknowledgements

Funding was provided by the U.S. Department of Energy through Contract No. DEAC36-08GO28308 FPACE II: Approaching the S-Q Limit with Epitaxial CdTe.

References

[1]M.A. Green, K. Emery, Y. Hishikawa, W. Warta, E.D. Dunlop, Solar cell efficiency tables (version 48), Prog. Photovolt. Res. Appl. 24 (2016) 905–913. doi:10.1002/pip.2788.

[2]M. Gloeckler, A.L. Fahrenbruch, J.R. Sites, Numerical modeling of CIGS and CdTe solar cells: setting the baseline, in: Proc. 3rd World Conf. Photovolt. Energy Convers. 2003, 2003: p. 491–494 Vol.1.

[3]T.A. Gessert, S.-H. Wei, J. Ma, D.S. Albin, R.G. Dhere, J.N. Duenow, D. Kuciauskas, A. Kanevce, T.M. Barnes, J.M. Burst, W.L. Rance, M.O. Reese, H.R. Moutinho, Research strategies toward improving thin-film CdTe photovoltaic devices beyond 20% conversion efficiency, Sol. Energy Mater. Sol. Cells. 119 (2013) 149–155. doi:10.1016/j.solmat.2013.05.055.

Pursuant to the DOE Public Access Plan, this document represents the authors' peer-reviewed, accepted manuscript. The published version of the article is available from the relevant publisher.

[4]J. Perrenoud, L. Kranz, C. Gretener, F. Pianezzi, S. Nishiwaki, S. Buecheler, A.N. Tiwari, A comprehensive picture of Cu doping in CdTe solar cells, J. Appl. Phys. 114 (2013) 174505. doi:10.1063/1.4828484.

[5]W. Lei, J. Antoszewski, L. Faraone, Progress, challenges, and opportunities for HgCdTe infrared materials and detectors, Appl. Phys. Rev. 2 (2015) 41303. doi:10.1063/1.4936577.

[6]J. Ma, D. Kuciauskas, D. Albin, R. Bhattacharya, M. Reese, T. Barnes, J.V. Li, T. Gessert, S.-H. Wei, Dependence of the Minority-Carrier Lifetime on the Stoichiometry of CdTe Using Time-Resolved Photoluminescence and First-Principles Calculations, Phys. Rev. Lett. 111 (2013) 67402. doi:10.1103/PhysRevLett.111.067402.

[7]J.M. Burst, J.N. Duenow, D.S. Albin, E. Colegrove, M.O. Reese, J.A. Aguiar, C.-S. Jiang, M.K. Patel, M.M. Al-Jassim, D. Kuciauskas, S. Swain, T. Ablekim, K.G. Lynn, W.K. Metzger, CdTe solar cells with open-circuit voltage breaking the 1 V barrier, Nat. Energy. 1 (2016) 16015. doi:10.1038/nenergy.2016.15.

[8]S.-H. Wei, S.B. Zhang, Chemical trends of defect formation and doping limit in II-VI semiconductors:\quad{}The case of CdTe, Phys. Rev. B. 66 (2002) 155211. doi:10.1103/PhysRevB.66.155211.

[9]E. Colegrove, S.P. Harvey, J.-H. Yang, J.M. Burst, D.S. Albin, S.-H. Wei, W.K. Metzger, Phosphorus Diffusion Mechanisms and Deep Incorporation in Polycrystalline and Single-Crystalline CdTe, Phys. Rev. Appl. 5 (2016) 54014. doi:10.1103/PhysRevApplied.5.054014.

[10]R. Triboulet, P. Siffert, CdTe and Related Compounds; Physics, Defects, Hetero- and Nano-structures, Crystal Growth, Surfaces and Applications: Physics, CdTe-based Nanostructures, CdTe-based Semimagnetic Semiconductors, Defects, Elsevier, 2009.

[11]H.-J. Lugauer, A. Waag, L. Worschech, W. Ossau, G. Landwehr, Generation of atomic group V materials for the p-type doping of wide gap II–VI semiconductors using a novel plasma cracker, J. Cryst. Growth. 161 (1996) 86–89. doi:10.1016/0022-0248(95)00673-7.

[12]M. Boukerche, P.S. Wijewarnasuriya, S. Sivananthan, I.K. Sou, Y.J. Kim, K.K. Mahavadi, J.P. Faurie, The doping of mercury cadmium telluride grown by molecular-beam epitaxy, J. Vac. Sci. Technol. Vac. Surf. Films. 6 (1988) 2830–2833. doi:10.1116/1.575610.

[13]J.E. Hails, S.J.C. Irvine, D.J. Cole-Hamilton, J. Giess, M.R. Houlton, A. Graham, As Doping in (Hg,Cd)Te: An Alternative Point of View, J. Electron. Mater. 37 (2008) 1291–1302. doi:10.1007/s11664-008-0452-1.

[14]J.H. Park, S. Farrell, R. Kodama, C. Blissett, X. Wang, E. Colegrove, W.K. Metzger, T.A. Gessert, S. Sivananthan, Incorporation and Activation of Arsenic Dopant in Single-Crystal CdTe Grown on Si

Pursuant to the DOE Public Access Plan, this document represents the authors' peer-reviewed, accepted manuscript. The published version of the article is available from the relevant publisher.

by Molecular Beam Epitaxy, J. Electron. Mater. 43 (2014) 2998–3003. doi:10.1007/s11664-014-3173-7.

[15] S. Farrell, T. Barnes, W.K. Metzger, J.H. Park, R. Kodama, S. Sivananthan, In Situ Arsenic Doping of CdTe/Si by Molecular Beam Epitaxy, J. Electron. Mater. 44 (2015) 3202–3206. doi:10.1007/s11664-015-3913-3.

[16] J.W. Garland, C. Grein, S. Sivananthan, Arsenic p-Doping of HgCdTe Grown by Molecular Beam Epitaxy (MBE): A Solved Problem?, J. Electron. Mater. Warrendale. 42 (2013) 3331–3336. doi:http://dx.doi.org/10.1007/s11664-013-2739-0.

[17] M.A. Berding, A. Sher, Amphoteric behavior of arsenic in HgCdTe, Appl. Phys. Lett. 74 (1999) 685–687. doi:10.1063/1.122987.

[18] H.R. Vydyanath, Amphoteric behaviour of group V dopants in (Hg, Cd)Te, Semicond. Sci. Technol. 5 (1990) S213. doi:10.1088/0268-1242/5/3S/047.

[19] H.F. Schaake, On the kinetics of the activation of arsenic as a p-type dopant in Hg1−xCdxTe, J. Electron. Mater. 30 (2001) 789–793. doi:10.1007/BF02665874.

[20] D. Chandra, D.F. Weirauch, H.F. Schaake, M.A. Kinch, F. Aqariden, C.F. Wan, H.D. Shih, Growth of very low arsenic-doped HgCdTe, J. Electron. Mater. 34 (2005) 963–967. doi:10.1007/s11664-005-0051-3.

[21] X. Biquard, I. Alliot, P. Ballet, Extended x-ray absorption fine structure study of arsenic in HgCdTe: p-type doping linked to nonsubstitutional As incorporation in an unknown AsHg8 structure, J. Appl. Phys. 106 (2009) 103501. doi:10.1063/1.3255989.

[22] P. Ballet, B. Polge, X. Biquard, I. Alliot, Extended X-ray Absorption Fine Structure Investigation of Arsenic in HgCdTe: the Effect of the Activation Anneal, J. Electron. Mater. 38 (2009) 1726–1732. doi:10.1007/s11664-009-0810-7.

[23] F. Gemain, I.C. Robin, S. Brochen, P. Ballet, O. Gravrand, G. Feuillet, Arsenic complexes optical signatures in As-doped HgCdTe, Appl. Phys. Lett. 102 (2013) 142104. doi:10.1063/1.4801500.

[24] R.B. Fair, Rapid Thermal Processing: Science and Technology, Academic Press, 2012.

[25] J. Li, D.R. Diercks, T.R. Ohno, C.W. Warren, M.C. Lonergan, J.D. Beach, C.A. Wolden, Controlled activation of ZnTe:Cu contacted CdTe solar cells using rapid thermal processing, Sol. Energy Mater. Sol. Cells. 133 (2015) 208–215. doi:10.1016/j.solmat.2014.10.045.

[26] M. Zandian, A.C. Chen, D.D. Edwall, J.G. Pasko, J.M. Arias, p-type arsenic doping of Hg1−xCdxTe by molecular beam epitaxy, Appl. Phys. Lett. 71 (1997) 2815–2817. doi:10.1063/1.120144.

[27] A.C. Chen, M. Zandian, D.D. Edwall, R.E.D. Wames, P.S. Wijewarnasuriya, J.M. Arias, S. Sivananthan, M. Berding, A. Sher, MBE growth and characterization of in situ arsenic doped HgCdTe, J. Electron. Mater. 27 (1998) 595–599. doi:10.1007/s11664-998-0021-7.

Pursuant to the DOE Public Access Plan, this document represents the authors' peer-reviewed, accepted manuscript. The published version of the article is available from the relevant publisher.

[28]P.S. Wijewarnasuriya, S. Sivananthan, Arsenic incorporation in HgCdTe grown by molecular beam epitaxy, Appl. Phys. Lett. 72 (1998) 1694–1696. doi:10.1063/1.121154.

[29]A. Nagaoka, K.-B. Han, S. Misra, T. Wilenski, T.D. Sparks, M.A. Scarpulla, Growth and characterization of Arsenic doped CdTe single crystals grown by Cd-solvent traveling-heater method, J. Cryst. Growth. 467 (2017) 6–11. doi:10.1016/j.jcrysgro.2017.03.002.

[30]C.H. Park, D.J. Chadi, Bulk Lattice Instability in II-VI Semiconductors and Its Effect on Impurity Compensation, Phys. Rev. Lett. 75 (1995) 1134–1137. doi:10.1103/PhysRevLett.75.1134.

[31]D.J. Chadi, Predictor of p-type doping in II-VI semiconductors, Phys. Rev. B. 59 (1999) 15181–15183. doi:10.1103/PhysRevB.59.15181.

[32]J.-H. Yang, W.-J. Yin, J.-S. Park, J. Burst, W.K. Metzger, T. Gessert, T. Barnes, S.-H. Wei, Enhanced p-type dopability of P and As in CdTe using non-equilibrium thermal processing, J. Appl. Phys. 118 (2015) 25102. doi:10.1063/1.4926748.

[33]J.-H. Yang, W.-J. Yin, J.-S. Park, J. Ma, S.-H. Wei, Review on first-principles study of defect properties of CdTe as a solar cell absorber, Semicond. Sci. Technol. 31 (2016) 83002. doi:10.1088/0268-1242/31/8/083002.

[34]T. Ablekim, S.K. Swain, W.-J. Yin, K. Zaunbrecher, J. Burst, T.M. Barnes, D. Kuciauskas, S.-H. Wei, K.G. Lynn, Self-compensation in arsenic doping of CdTe, Sci. Rep. 7 (2017). doi:10.1038/s41598-017-04719-0.

[35]Y. Marfaing, Impurity doping and compensation mechanisms in CdTe, Thin Solid Films. 387 (2001) 123–128. doi:10.1016/S0040-6090(00)01717-X.

[36]H. Duan, Y.Z. Dong, J. Luo, Y. Huang, X.S. Chen, W. Lu, Sources of carrier compensation in arsenic-doped HgCdTe, J. Phys. Chem. Solids. 74 (2013) 57–64. doi:10.1016/j.jpcs.2012.07.019.

[37]V. Barrioz, Y.Y. Proskuryakov, E.W. Jones, J.D. Major, S.J.C. Irvine, K. Durose, D.A. Lamb, Highly Arsenic Doped CdTe Layers for the Back Contacts of CdTe Solar Cells, MRS Online Proc. Libr. Arch. 1012 (2007). doi:10.1557/PROC-1012-Y12-08.

[38]S. Plissard, G. Giusti, B. Polge, P. Ballet, A. Million, X. Biquard, E. Molva, J. Barnes, P. Holliger, Extended X-Ray Absorption Fine Structure Study of Arsenic in HgCdTe, J. Electron. Mater. 36 (2007) 919–924. doi:10.1007/s11664-007-0133-5.

[39]L. Svob, Y. Marfaing, B. Clerjaud, D. Côte, A. Lebkiri, R. Druilhe, A. Lusson, C. Grattepain, Annealing kinetics of hydrogenated As acceptors in MOVPE grown CdTe, Semicond. Sci. Technol. 13 (1998) 79. doi:10.1088/0268-1242/13/1/012.

[40]D. Blavette, S. Duguay, Investigation of dopant clustering and segregation to defects in semiconductors using atom probe tomography, J. Appl. Phys. 119 (2016) 181502. doi:10.1063/1.4948238.

Pursuant to the DOE Public Access Plan, this document represents the authors' peer-reviewed, accepted manuscript. The published version of the article is available from the relevant publisher.

[41]J. Chai, K.-K. Lee, K. Doyle, J.H. Dinan, T.H. Myers, Growth of Lattice-Matched ZnTeSe Alloys on (100) and (211)B GaSb, J. Electron. Mater. 41 (2012) 2738–2744. doi:10.1007/s11664-012-2054-1.

[42]J. Moseley, M.M. Al-Jassim, H.L. Guthrey, J.M. Burst, J.N. Duenow, R.K. Ahrenkiel, W.K. Metzger, Cathodoluminescence spectrum imaging analysis of CdTe thin-film bevels, J. Appl. Phys. 120 (2016) 105704. doi:10.1063/1.4962286.

[43]K. Thompson, D. Lawrence, D.J. Larson, J.D. Olson, T.F. Kelly, B. Gorman, In situ site-specific specimen preparation for atom probe tomography, Ultramicroscopy. 107 (2007) 131–139. doi:10.1016/j.ultramic.2006.06.008.

[44]D.R. Diercks, B.P. Gorman, Nanoscale Measurement of Laser-Induced Temperature Rise and Field Evaporation Effects in CdTe and GaN, J. Phys. Chem. C. 119 (2015) 20623–20631. doi:10.1021/acs.jpcc.5b02126.

[45]B.P. Gorman, A. Puthucode, D.R. Diercks, M.J. Kaufman, Cross-correlative TEM and atom probe analysis of partial crystallisation in NiNbSn metallic glasses, Mater. Sci. Technol. 24 (2008) 682–688. doi:10.1179/174328408X293595.

[46]B. Gorman, D. Diercks, N. Salmon, E. Stach, G. Amador, C. Hartfield, Hardware and techniques for cross-correlative TEM and atom probe analysis, Microsc. Today. 16 (2008) 42–47.

[47]E. Colegrove, B. Stafford, W. Gao, T. Gessert, S. Sivananthan, Arsenic doped heteroepitaxial CdTe by MBE for applications in thin-film photovoltaics, in: 2014 IEEE 40th Photovolt. Spec. Conf. PVSC, 2014: pp. 3261–3265. doi:10.1109/PVSC.2014.6925632.

[48]M.K. Miller, THE EFFECTS OF LOCAL MAGNIFICATION AND TRAJECTORY ABERRATIONS ON ATOM PROBE ANALYSIS, J. Phys. Colloq. 48 (1987) C6-565-C6-570. doi:10.1051/jphyscol:1987692.

[49]F. De Geuser, W. Lefebvre, F. Danoix, F. Vurpillot, B. Forbord, D. Blavette, An improved reconstruction procedure for the correction of local magnification effects in three-dimensional atom-probe, Surf. Interface Anal. 39 (2007) 268–272. doi:10.1002/sia.2489.

[50]S.P. Harvey, G. Teeter, H. Moutinho, M.M. Al-Jassim, Direct evidence of enhanced chlorine segregation at grain boundaries in polycrystalline CdTe thin films via three-dimensional TOF-SIMS imaging, Prog. Photovolt. Res. Appl. 23 (2015) 838–846. doi:10.1002/pip.2498.

[51]K.N. Zaunbrecher, D. Kuciauskas, C.H. Swartz, P. Dippo, M. Edirisooriya, O.S. Ogedengbe, S. Sohal, B.L. Hancock, E.G. LeBlanc, P.A.R.D. Jayathilaka, T.M. Barnes, T.H. Myers, Impact of extended defects on recombination in CdTe heterostructures grown by molecular beam epitaxy, Appl. Phys. Lett. 109 (2016) 91904. doi:10.1063/1.4961989.

Pursuant to the DOE Public Access Plan, this document represents the authors' peer-reviewed, accepted manuscript. The published version of the article is available from the relevant publisher.

[52]G. Burton, D.R. Diercks, B.P. Gorman, Nanoscale effects of arsenic incorporation in CdTe grown by molecular beam epitaxy, in: 2016 IEEE 43rd Photovolt. Spec. Conf. PVSC, 2016: pp. 3015–3017. doi:10.1109/PVSC.2016.7750217.

[53]G.L. Burton, D.R. Diercks, B.P. Gorman, Dopant and Interfacial Analysis of Epitaxial CdTe Using Atom Probe Tomography, Microsc. Microanal. 21 (2015) 693–694. doi:10.1017/S1431927615004262.

Pursuant to the DOE Public Access Plan, this document represents the authors' peer-reviewed, accepted manuscript. The published version of the article is available from the relevant publisher.

Tables

Table I. Overall doping concentrations measured globally by SIMS and locally by APT as well as more detailed information about clusters found in APT analysis

Sample	SIMS average As incorporation (cm^{-3})	APT As overall concentration (cm^{-3})	V_{avg} Cluster (nm^3)	As Inside Clusters (%)	As Outside Clusters (%)
Unannealed	$7.68x10^{19}$	$3.08x10^{19}$	28.05	24.65	75.35
Ampoule	$1.67x10^{19}$	$4.10x10^{19}$	49.58	42.99	57.01
RTP 550°C	…	$1.36x10^{19}$	116.6	82.2	17.80
RTP 600°C	$2.19x10^{19}$	$3.97x10^{18}$	125.1	93.33	6.67

Pursuant to the DOE Public Access Plan, this document represents the authors' peer-reviewed, accepted manuscript. The published version of the article is available from the relevant publisher.

Figure Captions

Figure 1. (a) SEM image of the unannealed sample, showing a hillock. (b) is the average CL spectrum over the scanned area. (c) SEM image of RTP annealed As:CdTe surface and (d) is the average CL spectrum over the scanned area. The scale bars in (a) and (c) are 4 µm.

Figure 2. a) SIMS measurements and b) APT measurements of As concentration profiles in the unannealed, ampoule annealed and RTP 600 °C annealed samples. The profile for the RTP 550 °C annealed sample is also shown in (b).

Figure 3. Atom probe results showing As cluster formation. APT reconstruction of a) unannealed b) ampoule annealed c) RTP 550 °C annealed and d) RTP 600 °C samples showing 3.2 atomic percent arsenic isoconcentration surfaces in purple and a fraction of the Te ions in green (Other species are omitted from the image for clarity). Axes units are in nm; selected area of the APT reconstruction of the ampoule annealed sample from (b) showing planar features viewed e) along the *z*-axis and f) from the bottom of the specimen.

Figure 4. a) APT reconstruction of the RTP 550 °C annealed sample showing cluster formation on a closer scale. Arsenic 3.2% isoconcentration surfaces in purple and a fraction of the Te ions in green, as in Figure 3 (a)-(d). The cylindrical grey region of interest through one of the arsenic isoconcentration surfaces is representative of the volumes analyzed for 1D concentration profiles for the b) unannealed, c) RTP 550 °C annealed and d) RTP 600 °C annealed samples.

Figure 5. a) High Angle Annular Dark Field (HAADF) Scanning Transmission Electron Micrograph of an APT specimen prepared from the 550 °C RTP annealed sample b) magnified area of the APT specimen shown by the blue box in (a) and c) arsenic EDS map of the same region as (b). Circled regions in (b) and

Pursuant to the DOE Public Access Plan, this document represents the authors' peer-reviewed, accepted manuscript. The published version of the article is available from the relevant publisher.

(c) represent As enriched areas where the white dotted areas are ~1 at. % As, enriched in Cd, and deficient in Te and the red dotted circles are ~4 at. % As, enriched in Te and deficient in Cd. Scale bar is 30 nm.

Supplemental Information

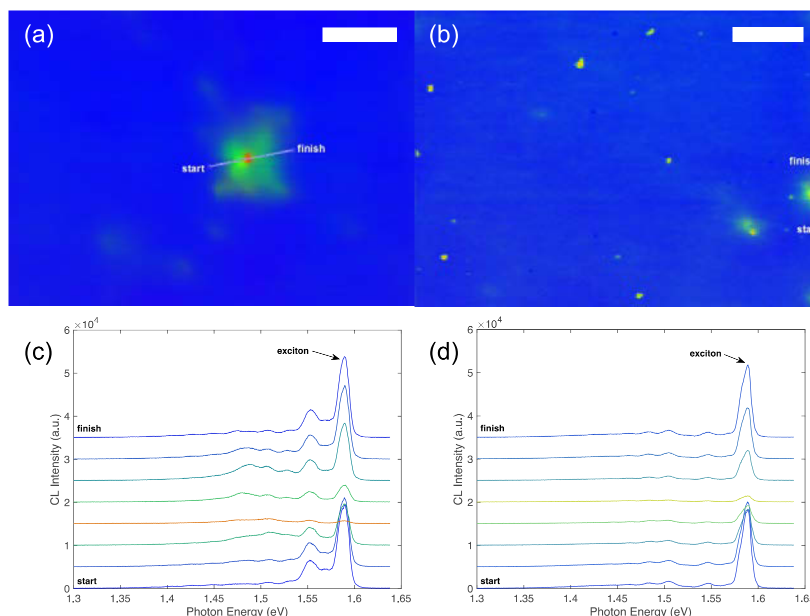

Supplemental Figure1 (a) CLSI false-color map of unannealed As:CdTe surface The spectra for the linescan in (a) are plotted in (c). (b) CLSI false-color map of RTP annealed As:CdTe surface The spectra for the linescan in (b) are plotted in (d).The scale bar in (a) and (b) is 4 μm.

CLSI false color maps

To make the false-color maps, all 40,000 (200×200) spectra were normalized by their spectral area and then mapped onto red-green-blue (RGB) colors according to: blue=1.65−1.56 eV, green=1.56−1.46 eV, and red=1.46−1.30 eV. The blue color in CLSI maps indicates exciton-dominant emission. The green/yellow/red spots indicate an increase in the relative intensity of deeper donor-acceptor pair (DAP) and electron-to-acceptor (eA^0) transitions but reduced intensity overall. By comparison to the SEM images, these spots are present near a hillock in Fig. 1(a) and debris in Fig. 1(b), likely due to increased non-radiative recombination or a reduction in the injection density. These low-temperature CLSI false color map results show the uniformity in doping across the samples.

Pursuant to the DOE Public Access Plan, this document represents the authors' peer-reviewed, accepted manuscript. The published version of the article is available from the relevant publisher.